

Emergence of rotational bands in *ab initio* no-core configuration interaction calculations of light nuclei

M. A. Caprio^a, P. Maris^b, J. P. Vary^b

^aDepartment of Physics, University of Notre Dame, Notre Dame, Indiana 46556-5670, USA

^bDepartment of Physics and Astronomy, Iowa State University, Ames, Iowa 50011-3160, USA

Abstract

The emergence of rotational bands is observed in no-core configuration interaction (NCCI) calculations for the odd-mass Be isotopes ($7 \leq A \leq 13$) with the JISP16 nucleon-nucleon interaction, as evidenced by rotational patterns for excitation energies, quadrupole moments, and $E2$ transitions. Yrast and low-lying excited bands are found. The results demonstrate the possibility of well-developed rotational structure in NCCI calculations using a realistic nucleon-nucleon interaction.

Keywords: No-core configuration interaction, Nuclear rotation, JISP16

PACS: 21.60.Cs, 21.10.-k, 21.10.Re, 27.20.+n

1. Introduction

Nuclei exhibit a wealth of collective phenomena, including clustering, rotation, and pairing [1–3]. Collective dynamics have been extensively modeled in phenomenological descriptions [1, 3–5]. Some forms of collectivity may also be obtained microscopically in the conventional (valence) shell model, *e.g.*, Elliott SU(3) rotation [6, 7]. However, observing the emergence of collective phenomena directly from first principles — that is, in a fully *ab initio* calculation of the nucleus, as a many-body system in which all the constituent protons and neutrons participate, with realistic interactions — remains as an outstanding challenge.

Recent developments in large-scale calculations have brought significant progress in the *ab initio* description of light nuclei [8–12]. In *ab initio* no-core configuration interaction (NCCI) approaches — such as the no-core shell model (NCSM) [11, 13–16], no-core Monte Carlo shell model (MCSM) [17], or no-core full configuration (NCFC) [18] methods — the nuclear many-body bound-state eigenproblem is formulated as a matrix diagonalization problem. The Hamiltonian is represented with respect to a basis of antisymmetrized products of single-particle states, generally harmonic oscillator states, and the problem is solved for the full system of A nucleons, *i.e.*, with no inert core. In practice, such calculations must be carried out in a finite space, obtained by truncating the many-body basis according to a maximum allowed number N_{\max} of oscillator excitations above the lowest oscillator configuration (*e.g.*, Ref. [11]). With increasing N_{\max} , the results converge towards those which would be achieved in the full, infinite-dimensional space for the many-body system.

Computational restrictions limit the extent to which converged calculations can be obtained for the observables needed for the identification of collective phenomena. In particular, the observables most indicative of rotational collectivity — $E2$

matrix elements — present special challenges for convergence in an NCCI approach [19, 20], due to their sensitivity to the large-radius asymptotic portions of the nuclear wave function. Nonetheless, some promising suggestions of collective phenomena, *e.g.*, deformation and clustering, have already been obtained in *ab initio* calculations [20–25].

In this letter, we observe the emergence of collective rotation in *ab initio* NCCI calculations for the Be isotopes, using the realistic JISP16 nucleon-nucleon interaction [26]. Evidence for rotational band structure is found in the calculated excitation energies, quadrupole moments, and $E2$ transition matrix elements. In NCCI calculations of the even-mass Be nuclei, yrast sequences of angular momenta 0, 2, 4, ... arise with calculated properties resembling those of $K = 0$ ground-state rotational bands (see Ref. [27] for a preliminary report of comparable results for ^{12}C). However, the most distinctive, well-developed, and systematic rotational band structures are observed in calculations for odd-mass nuclei. Given the same range of excitation energies and angular momenta, the low-lying $\Delta J = 1$ bands in the odd-mass nuclei provide a richer set of energy and electromagnetic observables. We therefore focus here on the odd-mass Be isotopes, specifically, with $7 \leq A \leq 13$. After a brief review of the properties expected in nuclear rotational structure (Sec. 2), the results for rotational bands in NCCI calculations of these Be isotopes are presented (Sec. 3). Preliminary results for ^9Be were reported in Ref. [25].

2. Rotation

We first review nuclear collective rotation and its expected signatures [1, 3]. Under the assumption of adiabatic separation of the rotational degree of freedom, a nuclear state may be described in terms of an *intrinsic state*, as viewed in the non-inertial intrinsic frame, together with the rotational motion of

this intrinsic frame. For axially symmetric structure, in particular, the intrinsic state $|\phi_K\rangle$ is characterized by definite angular momentum projection K along the intrinsic symmetry axis. The full nuclear state $|\psi_{JKM}\rangle$, with total angular momentum J and projection M , then has the form

$$|\psi_{JKM}\rangle = \left[\frac{2J+1}{16\pi^2(1+\delta_{K0})} \right]^{1/2} \int d\vartheta [\mathcal{D}_{MK}^J(\vartheta)|\phi_K; \vartheta\rangle + (-)^{J+K} \mathcal{D}_{M-K}^J(\vartheta)|\phi_{\bar{K}}; \vartheta\rangle], \quad (1)$$

where ϑ represents the Euler angles for rotation of the intrinsic state, and $|\phi_{\bar{K}}\rangle$ is the \mathcal{R}_2 -conjugate intrinsic state, which has angular momentum projection $-K$ along the symmetry axis.

The most recognizable features in the spectroscopy of rotational states reside not in the states taken individually but in the relationships among the different states $|\psi_{JKM}\rangle$ sharing the same intrinsic state $|\phi_K\rangle$. These states constitute members of a rotational band, with angular momenta $J = K, K+1, \dots$, except with only even J (or only odd J , depending upon the intrinsic \mathcal{R}_2 symmetry) for $K=0$ bands. Within a rotational band, energies follow the pattern

$$E(J) = E_0 + AJ(J+1), \quad (2)$$

where, in terms of the moment of inertia \mathcal{J} about an axis perpendicular to the symmetry axis, $A \equiv \hbar^2/(2\mathcal{J})$. For $K=1/2$ bands, the Coriolis contribution to the kinetic energy results in an energy staggering given by

$$E(J) = E_0 + A[J(J+1) + a(-)^{J+1/2}(J+\frac{1}{2})], \quad (3)$$

where a is the Coriolis decoupling parameter. Reduced matrix elements $\langle\psi_{J_f K}||Q_2||\psi_{J_i K}\rangle$ of the electric quadrupole operator Q_2 between states within a band are entirely determined by the rotational structure, except for the overall normalization, which is proportional to the intrinsic quadrupole moment $eQ_0 \equiv (16\pi/5)^{1/2}\langle\phi_K|Q_{2,0}|\phi_K\rangle$. In particular, quadrupole moments within a band are obtained as

$$Q(J) = \frac{3K^2 - J(J+1)}{(J+1)(2J+3)} Q_0, \quad (4)$$

and reduced transition probabilities as

$$B(E2; J_i \rightarrow J_f) = \frac{5}{16\pi} (J_i K 2 0 | J_f K)^2 (eQ_0)^2. \quad (5)$$

In obtaining these results, Q_2 can be taken to be any operator of the form $Q_{2\mu} = \sum_{i=1}^A e_i r_i^2 Y_{2\mu}(\hat{\mathbf{r}}_i)$ and may therefore represent the electromagnetic $E2$ transition operator, mass quadrupole tensor, neutron quadrupole tensor, *etc.*, depending upon the choice of coefficients e_i (see Sec. 3).

3. Results

An NCCI calculation is defined by the interaction for the nuclear system and by the truncated many-body space in which the calculation is carried out. The present calculations use the

JISP16 interaction [26], which is a two-body interaction derived from neutron-proton scattering data and adjusted via a phase-shift equivalent transformation to describe light nuclei without explicit three-body interactions. The bare interaction is used, without renormalization to the truncated space [18]. The Coulomb interaction has been omitted from the Hamiltonian, to ensure exact conservation of isospin, thereby simplifying the spectrum. (The primary effect of the Coulomb interaction, when included, is to induce a shift in the overall binding energies, which is irrelevant to identification of rotational band structure.) These calculations are carried out for oscillator truncations ranging from $N_{\max} = 10$ for ${}^7\text{Be}$ to $N_{\max} = 7$ for ${}^{13}\text{Be}$, with basis oscillator $\hbar\Omega$ parameters near the variational minimum ($\hbar\Omega = 20\text{--}22.5$ MeV). The proton-neutron M -scheme code MFDn [28–30] has been used for the many-body calculations.

The calculated excitation energies for low-lying states of the odd-mass Be isotopes (with $7 \leq A \leq 13$) are shown in Figs. 1 and 2. For each nucleus, there are two parity spaces to consider, shown separately in these two figures (energies are taken relative to the lowest state of the same parity). We refer to the parity of the lowest allowed oscillator configuration (negative for ${}^{7,9,11}\text{Be}$, positive for ${}^{13}\text{Be}$) as the *natural parity* (Fig. 1) and that obtained by promoting one nucleon by one shell as the *unnatural parity* (Fig. 2). The NCCI bases for these spaces consist of states with even and odd numbers of oscillator excitations, respectively, above the lowest configuration. While the lowest unnatural parity states normally lie at significantly higher energy than those of natural parity, they are calculated to lie within a few MeV of the lowest natural parity states in the isotopes ${}^{9,11,13}\text{Be}$ [25], which are therefore included in Fig. 2. Note that parity inversion arises for ${}^{11}\text{Be}$, *i.e.*, the ground state is experimentally [31] in the unnatural parity space, and both spaces are near-degenerate in calculations at finite N_{\max} (see Ref. [11]). The minimal isospin ($T = T_z$) spectrum is shown in each case.

To facilitate identification of rotational bands, it is helpful to plot the calculated excitation energies with respect to $J(J+1)$, so that energies within an ideal rotational band would lie on a straight line — or, for $K=1/2$ bands, staggered about a straight line. For the candidate $K=1/2$ bands in Figs. 1 and 2, an energy fit is obtained by adjusting the parameters of (3) to the first three bandmembers (the remainder of the line is thus an extrapolation). For the remaining bands, a straight line fit of (2) to all bandmembers is shown.

The yrast and near-yrast states yield the most immediately recognizable sets of candidate bandmembers. Yrast rotational bands (with bandmembers indicated by solid black squares in Figs. 1 and 2) are found with $K=1/2$ except in the natural parity space of ${}^9\text{Be}$ [Fig. 1(b)], for which the yrast band has $K=3/2$. The density of states rapidly increases off the yrast line, hindering identification of candidate bands and furthermore suggesting that the rotational states may be fragmented by mixing with nearby states. Nonetheless, several excited candidate bands (indicated by solid red squares) can also be clearly identified, with $1/2 \leq K \leq 5/2$, once transition strengths have been taken into account.

For the yrast $K=1/2$ bands, as a result of Coriolis decou-

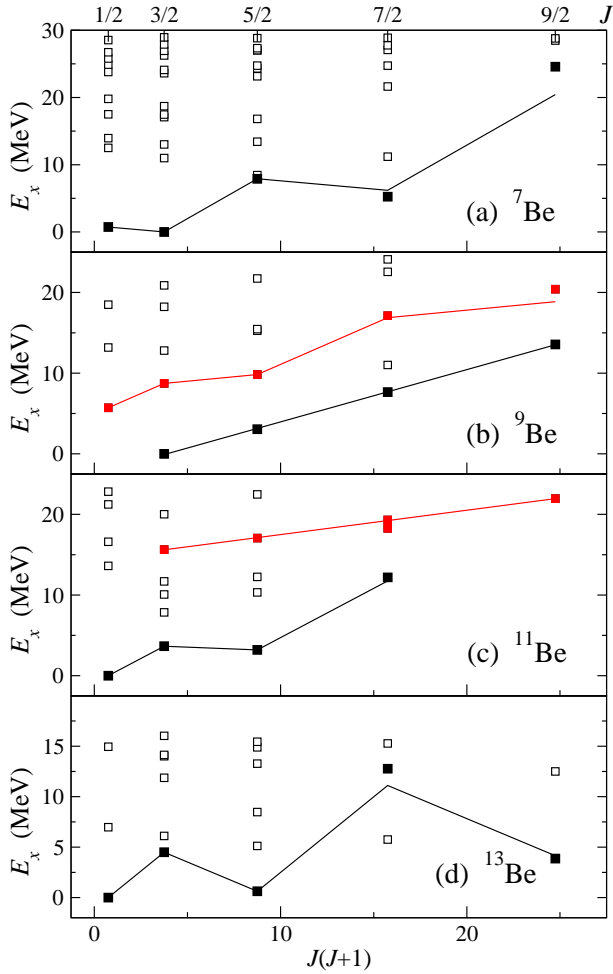


Figure 1: Excitation energies obtained for states in the *natural* parity spaces of the odd-mass Be isotopes: (a) ${}^7\text{Be}$, (b) ${}^9\text{Be}$, (c) ${}^{11}\text{Be}$, and (d) ${}^{13}\text{Be}$. Energies are plotted with respect to $J(J+1)$ to facilitate identification of rotational energy patterns, while the J values themselves are indicated at top. Filled symbols indicate candidate rotational bandmembers (black for yrast states and red for excited states). The lines indicate the corresponding best fits for rotational energies. Where quadrupole transition strengths indicate significant two-state mixing (see text), more than one state of a given J is indicated as a bandmember.

pling, it should be noted that alternate bandmembers are raised in energy into a region of higher density of states, which complicates identification and is conducive to fragmentation. The energy staggering in the calculated yrast band of the ${}^7\text{Be}$ natural parity space [Fig. 1(a)] — in which the $J = 3/2, 7/2, \dots$ levels are lowered, and the $J = 1/2, 5/2, \dots$ levels are raised — corresponds to a negative value of the decoupling parameter. Note that the staggering is sufficiently pronounced that the two lowest- J bandmembers are inverted, as experimentally observed for this nucleus [32]. Then, positive values of the decoupling parameter are instead obtained for the remaining $K = 1/2$ bands.

It is interesting to compare these *ab initio* results for the yrast bands in the natural parity spaces (Fig. 1) with the Nilsson model predictions [33, 34]. Specifically, the calculated yrast bands have $K = 1/2$ ($a \approx -1.4$) for ${}^7\text{Be}$, $K = 3/2$ for ${}^9\text{Be}$,

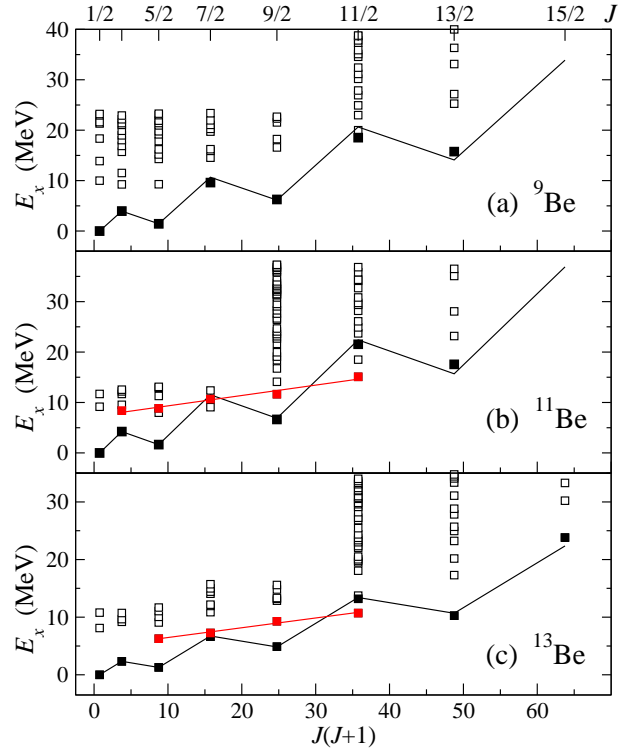


Figure 2: Excitation energies obtained for states in the *unnatural* parity spaces of the odd-mass Be isotopes: (a) ${}^9\text{Be}$, (b) ${}^{11}\text{Be}$, and (c) ${}^{13}\text{Be}$. Energies are plotted with respect to $J(J+1)$ to facilitate identification of rotational energy patterns, while the J values themselves are indicated at top. Filled symbols indicate candidate rotational bandmembers (black for yrast states and red for excited states). The lines indicate the corresponding best fits for rotational energies. Quadrupole transition strengths indicate significant but ambiguous two-state or multistate mixing for certain poorly-isolated bandmembers.

$K = 1/2$ ($a \approx +1.2$) for ${}^{11}\text{Be}$, and $K = 1/2$ ($a \approx +3.1$) for ${}^{13}\text{Be}$. The expected Nilsson $[Nn_z\Lambda\Omega]$ asymptotic quantum number assignments (see Fig. 5-1 of Ref. [3]) and corresponding Nilsson values of the decoupling parameter are $[110\frac{1}{2}]$ ($a \approx -1$) for ${}^7\text{Be}$, $[101\frac{3}{2}]$ for ${}^9\text{Be}$, $[101\frac{1}{2}]$ ($a \approx 0$) for ${}^{11}\text{Be}$, and $[220\frac{1}{2}]$ ($a \approx +1$) for ${}^{13}\text{Be}$. We see consistency not only in the K ($= \Omega$) quantum numbers for the band but also in the *qualitative* trend of the decoupling parameters for these bands. (The Nilsson values for a [33, 34] consider mixing of spherical orbitals only within a single spherical oscillator shell, which is sufficient for a weakly-deformed oscillator-like mean field. However, they should not be expected to provide *quantitative* accuracy for a nucleon in, say, the mean field produced by a double- α ${}^8\text{Be}$ core.)

The quadrupole moments for all states within the candidate bands are shown in Figs. 3 and 4, both for the yrast bands (black squares) and for the excited bands (red diamonds). The values are normalized to Q_0 , to facilitate comparison with the rotational predictions for $Q(J)/Q_0$ from (4) (shown as curves in each plot). The value of Q_0 used for normalization has in each case been obtained simply from the quadrupole moment of the lowest-energy bandmember of nonvanishing quadrupole moment. (Thus, for $K = 1/2$ bands, since the quadrupole mo-

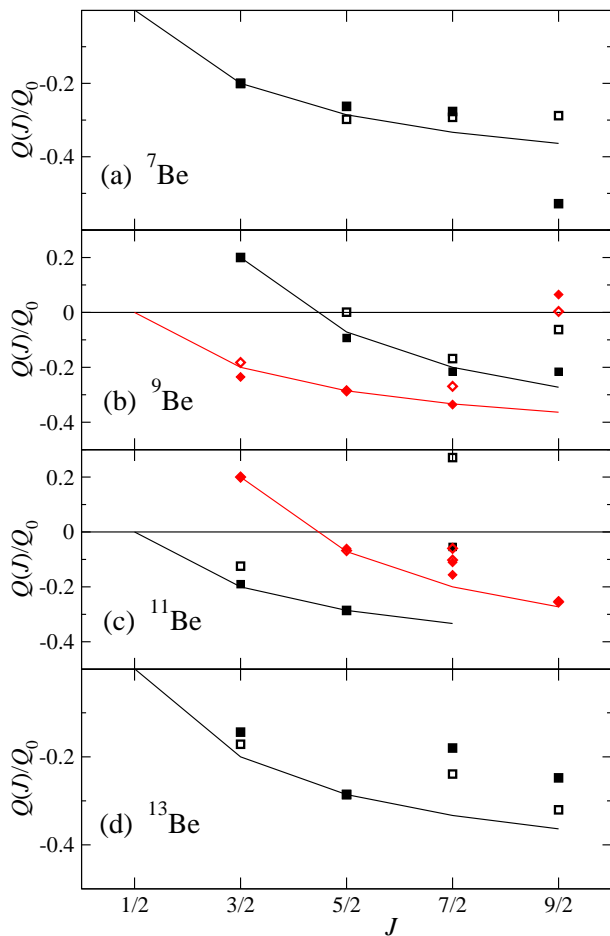


Figure 3: Quadrupole moments calculated for candidate bandmembers in the *natural* parity spaces of the odd-mass Be isotopes: (a) ${}^7\text{Be}$, (b) ${}^9\text{Be}$, (c) ${}^{11}\text{Be}$, and (d) ${}^{13}\text{Be}$. The states are as identified in Fig. 1 and are shown as black squares for yrast states or red diamonds for excited states. Filled symbols indicate proton quadrupole moments, and open symbols indicate neutron quadrupole moments. The curves indicate the theoretical values for a $K = 1/2$ or $K = 3/2$ rotational band, as appropriate, given by (4). Quadrupole moments are normalized to Q_0 , which is defined by either the $J = 3/2$ or $J = 5/2$ bandmember (see text).

ment of the $J = 1/2$ bandhead vanishes identically, either the $J = 3/2$ or $5/2$ bandmember is used for normalization, according to the staggering.) Quadrupole moments in Figs. 3 and 4 are calculated using both the proton (filled symbols) and neutron (open symbols) quadrupole tensors.¹

Finally, in-band transition strengths are shown in Fig. 5, again as obtained for both proton (solid symbols) and neutron (open symbols) quadrupole operators, and for $\Delta J = 2$ transitions (upper curves, solid) and $\Delta J = 1$ transitions (lower

¹The proton quadrupole tensor, defined as $Q_{2\mu,p} = \sum_{i=1}^Z r_{p,i}^2 Y_{2\mu}(\hat{\mathbf{r}}_{p,i})$, is the operator used in calculation of the physically observable electromagnetic moments and transitions. However, the rotational relations (4) and (5) are equally applicable to matrix elements of the neutron quadrupole tensor, $Q_{2\mu,n} = \sum_{i=1}^N r_{n,i}^2 Y_{2\mu}(\hat{\mathbf{r}}_{n,i})$. These therefore provide a valuable complementary set of observables for purposes of investigating whether or not the nuclear wave functions satisfy the conditions of adiabatic rotational separation, particularly relevant, due to the high neutron-proton asymmetry, in the neutron-rich Be isotopes.

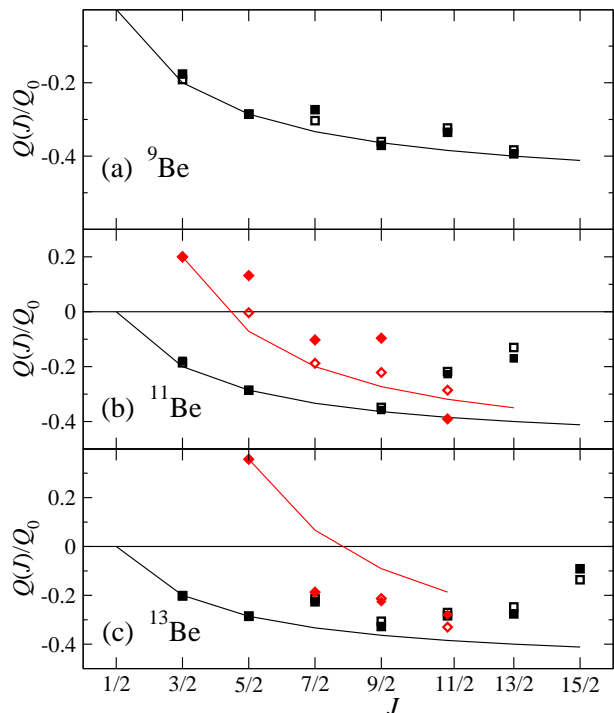


Figure 4: Quadrupole moments calculated for candidate bandmembers in the *unnatural* parity spaces of the odd-mass Be isotopes: (a) ${}^9\text{Be}$, (b) ${}^{11}\text{Be}$, and (c) ${}^{13}\text{Be}$. The states are as identified in Fig. 2 and are shown as black squares for yrast states or red diamonds for excited states. Filled symbols indicate proton quadrupole moments, and open symbols indicate neutron quadrupole moments. The curves indicate the theoretical values for a $K = 1/2$ or $K = 3/2$ rotational band, as appropriate, given by (4). Quadrupole moments are normalized to Q_0 , which is defined by either the $J = 3/2$ or $J = 5/2$ bandmember (see text).

curves, dashed). The various $K = 1/2$ bands are superposed in Fig. 5(a), and the $K = 3/2$ bands are shown in Fig. 5(b). Transition strengths are normalized as $B(E2; J \rightarrow J - \Delta J)/(eQ_0)^2$, for comparison with the rotational values from (5). The same Q_0 values are used as in Figs. 3 and 4, *i.e.*, obtained from $Q(3/2)$ or $Q(5/2)$. Therefore, no free normalization parameters remain for the $B(E2)$ strengths in Fig. 5. For instance, it may be observed that the values for $B(E2; 3/2 \rightarrow 1/2)/(eQ_0)^2$ in Fig. 5(a) cluster at the rotational value, indicating that the calculated $B(E2; 3/2 \rightarrow 1/2)$ strengths are in the proper relation to the calculated $Q(3/2)$ moment or $Q(5/2)$ moment, as appropriate, consistent with adiabatic rotation.

The level of resemblance between the calculated energies, quadrupole moments, and transition strengths for the candidate bands and the expected rotational values in Figs. 1–5, while clearly not perfect, indicates a remarkably clean separation of rotational and intrinsic degrees of freedom in these *ab initio* NCCI calculations. One should bear in mind that quadrupole moments of *arbitrarily* chosen states in the spectrum fluctuate not only in magnitude but also in sign, and that calculated $E2$ strengths among arbitrarily chosen pairs of states fluctuate by many orders of magnitude. (The $3/2 \rightarrow 1/2$ transitions in Fig. 5 are enhanced by factors of ~ 1.1 – 17 relative to the typical Weiskopf single-particle estimate [35].)

It is worth highlighting a few notable features from the band

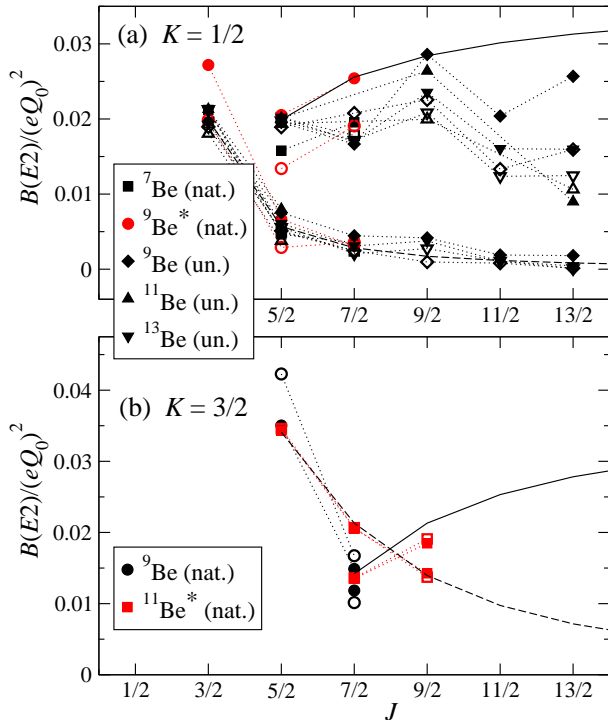


Figure 5: Transition $B(E2; J \rightarrow J-2)$ and $B(E2; J \rightarrow J-1)$ strengths calculated between candidate bandmembers, for bands with (a) $K = 1/2$ or (b) $K = 3/2$, in the odd-mass Be isotopes ${}^7\text{Be}$, ${}^9\text{Be}$, ${}^{11}\text{Be}$, and ${}^{13}\text{Be}$ (asterisks in the legend indicate excited bands). The curves indicate the theoretical values for $\Delta J = 2$ (upper curves, solid) and $\Delta J = 1$ (lower curves, dashed) transitions in a band of the given K , given by (5). Calculated transition strengths of the same ΔJ within a band are connected by dotted lines. Filled symbols indicate proton strengths, and open symbols indicate neutron strengths. Values are normalized to the same intrinsic quadrupole moment Q_0 as in Fig. 3 or 4. Where transition strengths indicate significant fragmentation of the rotational state over multiple calculated states, namely, for the ${}^{11}\text{Be}$ excited $J = 7/2$ state identified in Fig. 1(c), the $B(E2)$ values for transitions into or out of this state are summed.

structures in Figs. 1–5:

(1) The $K = 1/2$ yrast bands in the unnatural parity spaces (Fig. 2) can be traced to J values as high as $\sim 13/2$. For instance, for ${}^{13}\text{Be}$ [Fig. 2(c)], the energies of the $J = 7/2, 9/2, 11/2$, and $13/2$ bandmembers all agree with the rotational values, from (3), to within 0.4 MeV, and a $J = 15/2$ bandmember can also be reasonably identified (within 1.5 MeV of the rotational energy). The quadrupole moments [Fig. 4(c)] of the $J = 3/2$ and $J = 5/2$ bandmembers (the latter is used to determine Q_0 in the figure) are in the expected rotational ratio, from (4), to within 1.1% for protons or 0.4% for neutrons. The quadrupole moments for the higher bandmembers are highly consistent between protons and neutrons and have the expected sign, but they gradually fall off from the rotational values, approaching zero for the $J = 15/2$ bandmember.

(2) For the yrast and low-lying rotational bands in the natural parity spaces (Fig. 1), rotational behavior appears to terminate at generally lower angular momentum. For instance, for ${}^{11}\text{Be}$ [Fig. 1(c)], the $K = 1/2$ yrast band terminates at $J = 7/2$ on the basis of energies: the lowest calculated $J = 7/2$ state lies within 0.5 MeV of the expected energy extrapolated for an yrast

bandmember, but the lowest calculated $J = 9/2$ state is 11 MeV too high in energy to be an yrast bandmember. The terminating angular momentum expected in a simple valence p -shell or NCCI $N_{\text{max}} = 0$ description is, in fact, $J = 7/2$. The quadrupole moments [Fig. 3(c)] suggest that the viability of a rotational description may end even earlier, at $J = 5/2$. Similar comments may be made about the yrast and excited bands in ${}^7\text{Be}$ and ${}^9\text{Be}$ [Fig. 1(a,b)], where the quadrupole moments [Fig. 3(a,b)] are in close agreement with rotational values through $J = 7/2$, but then begin to deviate significantly at $J = 9/2$.

(3) To some extent in the quadrupole moments, but especially in the $\Delta J = 2$ transition strengths for the $K = 1/2$ bands [Fig. 5(a)], one may observe that the $E2$ matrix element strengths start at the expected rotational values for low J but then systematically fall off below the rotational values at higher J . This trend signals deviation from a strict *adiabatic* rotational picture, as described in Sec. 2, but it is also, at least qualitatively, in agreement with more microscopic treatments of nuclear rotation. Specifically, $E2$ matrix elements within an Elliott $SU(3)$ band decline in strength as band termination is approached (see discussion in Ref. [7]). A similar falloff can be obtained in $Sp(3, \mathbb{R})$ symplectic calculations [36] of rotational bands (see Fig. 6 of Ref. [37]). Whether or not such $SU(3)$ or $Sp(3, \mathbb{R})$ rotational mechanisms are at play in the present NCCI results awaits full analysis in an $SU(3)/Sp(3, \mathbb{R})$ symmetry-adapted implementation of the NCCI approach [38].

As we explore the interpretation of NCCI results in a rotational context, it is interesting to note that straightforward fragmentation of the rotational strength over two calculated levels can be observed for the $J = 7/2$ member of the excited band in the natural parity space of ${}^{11}\text{Be}$ [Fig. 1(c)]. Transitions into and out of this state are fragmented in the approximate proportion 0.4 : 0.6. However, the summed strengths, shown in Fig. 5(b), which combine the fragmented transitions involving this level, are in near-perfect agreement with rotational values.

We also note that a staggering may be observed in the $\Delta J = 2$ transition strengths, to a greater or lesser degree, for the various $K = 1/2$ bands [Fig. 5(a)]. Such staggering is in fact consistent with the adiabatic rotational picture, once the $\langle \phi_K | Q_{2,2K} | \phi_{\bar{K}} \rangle$ cross term in the rotational $E2$ matrix element, neglected in (5), is taken into account [see (6.38) of Ref. [1]]. In well-deformed rotor nuclei, this contribution is commonly ignored, on the presumption that $\langle \phi_K | Q_{2,0} | \phi_{\bar{K}} \rangle \sim Q_0$ is strongly enhanced while $\langle \phi_K | Q_{2,2K} | \phi_{\bar{K}} \rangle$ is of single-particle strength [1]. However, in light nuclei, where the collective enhancement is weaker, such a single-particle contribution may be expected to be nonnegligible in comparison, and to be of approximately the magnitude seen in Fig. 5(a).

4. Conclusion

The principal challenge in identifying collective structure in NCCI calculations with realistic interactions lies in the weak convergence of the relevant observables. Eigenvalues and other calculated observables are dependent upon both the truncation N_{max} and the oscillator length parameter (or $\hbar\Omega$) for the NCCI

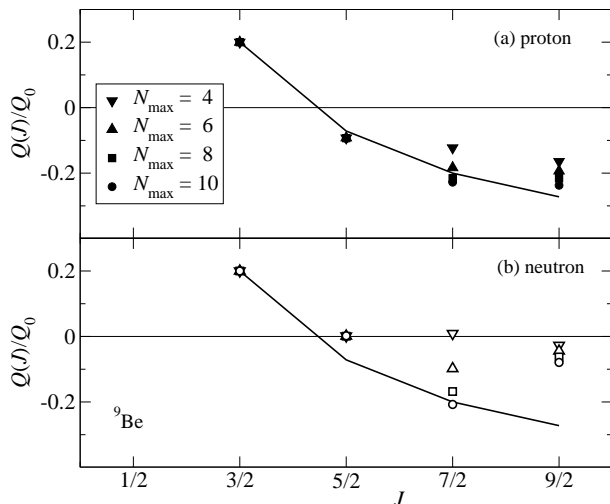


Figure 6: Relative quadrupole moments $Q(J)/Q_0$, calculated with the (a) proton and (b) neutron quadrupole tensor, for the $K = 3/2$ yrast band in the ${}^9\text{Be}$ natural parity space, from calculations with basis truncations $N_{\text{max}} = 4, 6, 8,$ and 10 . Since the normalization Q_0 is obtained in each case from $Q(3/2)$, the plotted values indicate the N_{max} dependence of the ratio $Q(J)/Q(3/2)$.

basis. Although it is possible to extrapolate the values of calculated observables to their values in the full, infinite space [18–20, 39, 40], such methods are still in their formative stages, especially for the crucial $E2$ observables. It is therefore particularly notable that quantitatively well-developed and robust signatures of rotation may be observed in the present results. That this is possible reflects the distinction between convergence of *individual* observables, taken singly, and convergence of *relative* properties, such as ratios of excitation energies or ratios of quadrupole matrix elements. It is these latter relative properties which are essential to identifying rotational dynamics and which are found to be sufficiently converged to yield stable rotational patterns at currently achievable N_{max} truncations, as illustrated in Fig. 6 for the $K = 3/2$ ground-state band of ${}^9\text{Be}$.

From the results of Sec. 3, it is seen that rotational structure is pervasive in *ab initio* NCCI calculations of light nuclei, occurring in the yrast and near-yrast regions of all the spectra considered for the Be isotopic chain. With suitable extrapolation methods in place, a salient test of *ab initio* calculations and interactions will then be quantitative prediction of collective rotational parameters, such as the intrinsic quadrupole moment, for direct comparison with experiment. One may observe that the present discussion represents a phenomenological rotational analysis, in the traditional experimental sense, but of a large set of observables taken from *ab initio* calculations of nuclei. Having full access to the calculated wavefunctions, we may also hope to extract information on the collective structure of the nuclear eigenstates from other measures of the wave function correlations, such as density distributions [20] and symmetry decompositions [41]. Natural questions include the origin of rotation in the Be isotopes — for instance, the extent to which it might arise from relative motion of alpha clusters or perhaps

from SU(3) rotation in an extended multi-shell valence space — and the relevance of some form of Nilsson-like strong-coupling picture for rotation in *ab initio* calculations of odd-mass light nuclei. Indeed, the proton and neutron density distributions found in Ref. [25] for the ground state of ${}^9\text{Be}$ suggest the emergence of two alpha clusters, with the additional neutron in a π orbital.

Acknowledgements

Discussions with A. O. Macchiavelli and P. Fallon are gratefully acknowledged. This work was supported by the Research Corporation for Science Advancement through the Cottrell Scholar program, by the US Department of Energy under Grants No. DE-FG02-95ER-40934, DE-FC02-09ER41582 (SciDAC/UNEDF), DESC0008485 (SciDAC/NUCLEI), and DE-FG02-87ER40371, and by the US National Science Foundation under Grant No. 0904782. Computational resources were provided by the National Energy Research Supercomputer Center (NERSC), which is supported by the Office of Science of the U.S. Department of Energy under Contract No. DE-AC02-05CH11231.

References

References

- [1] D. J. Rowe, *Nuclear Collective Motion: Models and Theory* (World Scientific, Singapore, 2010).
- [2] A. Bohr and B. R. Mottelson, *Nuclear Structure*, Vol. 1 (World Scientific, Singapore, 1998).
- [3] A. Bohr and B. R. Mottelson, *Nuclear Structure*, Vol. 2 (World Scientific, Singapore, 1998).
- [4] F. Iachello and A. Arima, *The Interacting Boson Model* (Cambridge University Press, Cambridge, 1987).
- [5] J. M. Eisenberg and W. Greiner, *Nuclear Theory*, 3rd ed., Vol. 1 (North-Holland, Amsterdam, 1987).
- [6] J. P. Elliott, Proc. R. Soc. London A 245 (1958) 128.
- [7] M. Harvey, Adv. Nucl. Phys. 1 (1968) 67.
- [8] S. C. Pieper, R. B. Wiringa, and J. Carlson, Phys. Rev. C 70 (2004) 054325.
- [9] T. Neff and H. Feldmeier, Nucl. Phys. A 738 (2004) 357.
- [10] G. Hagen, D. J. Dean, M. Hjorth-Jensen, T. Papenbrock, and A. Schwenk, Phys. Rev. C 76 (2007) 044305.
- [11] P. Navrátil, S. Quaglioni, I. Stetcu, and B. R. Barrett, J. Phys. G 36 (2009) 083101.
- [12] S. Bacca, N. Barnea, and A. Schwenk, Phys. Rev. C 86 (2012) 034321.
- [13] P. Navrátil, J. P. Vary, and B. R. Barrett, Phys. Rev. Lett. 84 (2000) 5728.
- [14] P. Navrátil, J. P. Vary, and B. R. Barrett, Phys. Rev. C 62 (2000) 054311.
- [15] J. P. Vary, P. Maris, E. Ng, C. Yang, and M. Sosonkina, J. Phys. Conf. Ser. 180 (2009) 012083.
- [16] B. R. Barrett, P. Navrátil, and J. P. Vary, Prog. Part. Nucl. Phys. (in press).
- [17] T. Abe, P. Maris, T. Otsuka, N. Shimizu, Y. Utsuno, and J. P. Vary, Phys. Rev. C 86 (2012) 054301.
- [18] P. Maris, J. P. Vary, and A. M. Shirokov, Phys. Rev. C 79 (2009) 014308.
- [19] S. K. Bogner, R. J. Furnstahl, P. Maris, R. J. Perry, A. Schwenk, and J. Vary, Nucl. Phys. A 801 (2008) 21.
- [20] C. Cockrell, J. P. Vary, and P. Maris, Phys. Rev. C 86 (2012) 034325.
- [21] R. B. Wiringa, S. C. Pieper, J. Carlson, and V. R. Pandharipande, Phys. Rev. C 62 (2000) 014001.
- [22] T. Neff and H. Feldmeier, Eur. Phys. J. Special Topics 156 (2008) 69.
- [23] Y. Kanada-En'yo, M. Kimura, and A. Ono, Prog. Exp. Theor. Phys. 2012 (2012) 01A202.
- [24] N. Shimizu, T. Abe, Y. Tsunoda, Y. Utsuno, T. Yoshida, T. M. M. Honma, and T. Otsuka, Prog. Exp. Theor. Phys. 2012 (2012) 01A205.

- [25] P. Maris, J. Phys. Conf. Ser. 402 (2012) 012031.
- [26] A. M. Shirokov, J. P. Vary, A. I. Mazur, and T. A. Weber, Phys. Lett. B 644 (2007) 33.
- [27] P. Maris, H. M. Aktulga, M. A. Caprio, U. V. Catalyurek, E. Ng, D. Orsypayev, H. Potter, E. Saule, M. Sosonkina, J. P. Vary, C. Yang, and Z. Zhou, J. Phys. Conf. Ser. 403 (2012) 012019.
- [28] P. Sternberg, E. G. Ng, C. Yang, P. Maris, J. P. Vary, M. Sosonkina, and H. V. Le, in *SC '08: Proceedings of the 2008 ACM/IEEE Conference on Supercomputing* (IEEE Press, Piscataway, NJ, 2008), Article No. 15.
- [29] P. Maris, M. Sosonkina, J. P. Vary, E. Ng, and C. Yang, Procedia Comput. Sci. 1 (2010) 97.
- [30] H. M. Aktulga, C. Yang, E. G. Ng, P. Maris, and J. P. Vary, in *Euro-Par 2012 Parallel Processing*, edited by C. Kaklamanis, T. Papatheodorou, and P. G. Spirakis (Springer-Verlag, Berlin, 2012), Lecture Notes in Computer Science Vol. 7484, p. 830.
- [31] F. Ajzenberg-Selove, Nucl. Phys. A 506 (1990) 1.
- [32] D. R. Tilley, C. M. Cheves, J. L. Godwin, G. M. Hale, H. M. Hofmann, J. H. Kelley, C. G. Sheu, and H. R. Weller, Nucl. Phys. A 708 (2002) 3.
- [33] S. G. Nilsson, Mat. Fys. Medd. Dan. Vid. Selsk. 29 (16) (1955).
- [34] B. R. Mottelson and S. G. Nilsson, Mat. Fys. Skr. Dan. Vid. Selsk. 1 (8) (1959).
- [35] V. F. Weisskopf, Phys. Rev. 83 (1951) 1073.
- [36] J. P. Draayer, K. J. Weeks, and G. Rosensteel, Nucl. Phys. A 413 (1984) 215.
- [37] D. J. Rowe, Rep. Prog. Phys. 48 (1985) 1419.
- [38] T. Dytrych, K. D. Sviratcheva, J. P. Draayer, C. Bahri, and J. P. Vary, J. Phys. G 35 (2008) 123101.
- [39] R. J. Furnstahl, G. Hagen, and T. Papenbrock, Phys. Rev. C 86 (2012) 031301.
- [40] S. A. Coon, M. I. Avetian, M. K. G. Kruse, U. van Kolck, P. Maris, and J. P. Vary, Phys. Rev. C 86 (2012) 054002.
- [41] T. Dytrych, K. D. Sviratcheva, C. Bahri, J. P. Draayer, and J. P. Vary, J. Phys. G 35 (2008) 095101.